Structural modifications of lanthanum silicate oxyapatite exposed to high water pressure

Aénor Pons, Jenny Jouin, Maggy Colas, Emilie Bechade, Pierre-Marie Geffroy, Mikhail Smirnov, Olivier Masson, Philippe Thomas, Isao Kagomiya, Toru Asaka, et al.

Structural modifications of lanthanum silicate oxyapatite exposed to high water pressure

Aénor Pons[a], Jenny Jouin[a], Maggy Colas[a], Emilie Béchade[a*], Pierre-Marie Geffroy[a], Mikhail Smirnov[f], Olivier Masson[a], Philippe Thomas[a], Isao Kagomiya[b], Toru Asaka[c], Koichiro Fukuda[c], Aneta Slodczyk[d e], Philippe Colomban[d e]

[a] *Science des Procédés Céramiques et de Traitements de Surface (SPCTS), CNRS UMR 7315, Centre Européen de la Céramique, 12 rue Atlantis, 87068 LIMOGES Cedex, France*

[b] *Department of Materials Science and Engineering, Nagoya Institute of Technology, Nagoya 466-8555, Japan*

[c] *Department of Environmental and Materials Engineering, Nagoya Institute of Technology, Nagoya 466-8555, Japan*

[d] *Sorbonne Universités, UPMC Univ Paris 06, UMR 8233, 4 Place Jussieu, 75005 Paris, France*

[e] *CNRS-IP2CT, UMR 8233, MONARIS, 4 Place Jussieu, 75005 Paris, France*

[f] *Department of Physics, Saint-Petersburg State University, 198504 Petrodvorets, Russia*

Abstract

Lanthanum silicate oxyapatite samples of initial compositions $La_{9.13}(SiO_4)_6O_{1.7}$, $La_{9.33}(SiO_4)_6O_2$ and $La_{9.60}(SiO_4)_6O_{2.4}$ were exposed to high water pressure in autoclave, in order to study the effects of initial oxygen stoichiometry and treatment duration on the protonation of these materials. TG analyses, done on very dense pellets (over 98.5%), showed that protonic species from the water vapour were successfully introduced into the bulk of the material. The sample showing the higher mass change after treatment was the one of initial composition $La_{9.60}(SiO_4)_6O_{2.4}$, after 84 hours of treatment at 550°C under 40 bars water pressure. The mass loss observed above 600°C (bulk species) is about 0.2% which is in good agreement with observed results on TG curves recorded on very dense (~99%) perovskite pellets (under He atmosphere and for approximate duration times). Furthermore, it was shown that the mass loss increases when protonation time rises (0.66% for 408 h), with a time limit beyond which the microstructure of the oxyapatite is no more stable (between 84 and 408h).

Rietveld refinement of the cell parameters and structural study by Raman spectroscopy presented some structural modifications (especially on La-$O5_{(channel)}$ bonds) which could be linked to the incorporation of protonic species. Indeed, it was shown that high water pressure treatment induced an increase of the cell volume (V~597.69 A to be compared with 587.69 A

for non-protonated La960) related to an increase of the a and b lattice parameters and an enlargement of the characteristic channels of oxyapatite.

Keywords: oxyapatite; powders solid-state reaction; fuel cells; SOFC; protonation; structure

*Corresponding author: emilie.bechade@unilim.fr

1. Introduction

The development of environment-friendly electrochemical applications and clean energy conversion systems, such as Solid Oxide Fuel Cells (SOFC), is nowadays attracting a great scientific interest [1,2].The most common material used as solid electrolyte in SOFC is oxide ion conducting yttria-stabilized zirconia (YSZ) [2,3]. However, current research aims to decrease the working temperature of SOFC down to intermediate temperatures (600-800°C) by using new oxide ion conductors with equivalent conductivity values than YSZ at 1000°C (above 0.1 $S.cm^{-1}$). Apatite-type lanthanum silicates of general formula $La_{9.33+x}(SiO_4)_6O_{2+3x/2}$, found by Nakayama *and al.* [4,5], are one of the most promising oxide ion conductors for application as electrolyte in Intermediate-Temperature SOFC (IT-SOFC) [5,6,7,8,9]. Their structure is based on a 3-dimensional organization of isolated silica tetrahedral and forms large lanthanum oxide tunnels oriented along the c-axis [10,11,12]. Such a structure can explain that oxyapatites exhibit high anisotropic conductivity in the c direction, which is increased by the incorporation of interstitial oxygen inside the large tunnels (formula with $x > 0$) [6,7,8,9,13,14,15]. The reactive diffusion method reported by Fukuda *and al.* [6,7,11,16] allows the elaboration of highly c-axis oriented lanthanum silicate apatite polycrystal material which exhibited high oxide ion conductivity values : 2.4×10^{-3} $S.cm^{-1}$ to 2.39×10^{-2} $S.cm^{-1}$ from 573 to 973 K with an activation energy of 0.35 eV (in agreement with the calculated migration energy of 0.32 eV linked to an original push-pull mechanism [14,17]).

Recent studies [18,19,20] show that the apatite structure could also enable the incorporation and conduction of protons. Thus, oxyapatite might be a new promising proton-conducting material for application as electrolyte in Proton Conducting SOFC (PC-SOFC)[21,22], which has the advantage of operating at lower temperatures (400-600°C). Contrary to anionic conduction, in the case of protonic conduction, the electrolyte material requires a moisturizing step, in order to enable the insertion and conduction of protons, which are not usually present in the material structure. The first works about the protonation of oxides, on the 1950s, has been performed on the reduction of ZnO materials which have shown the incorporation of protons in the oxide lattice [23]. Most studies, especially about (Ba, Sr)(Zr, Ce, Ti, Y)$O_{3-\delta}$ oxygen deficient perovskite materials [24,25,26,27,28,29,30] shows the complexity of water/proton insertion mechanism (called protonation) and the competition between surface and volume protonic species during the protonation step. Colomban *et al.* [25,26,27,28] found out that the pure and dense samples of (Ba, Sr)(Zr, Ce, Ti, Y)$O_{3-\delta}$ perovskites, under high pressures of decarbonated water and at high temperature (using an autoclave), promotes the creation of

volume protonic species, instead of surface water and surface hydroxycarbonate-type species (which must be avoided in the case of electrolyte materials of PC-SOFC).

Reactions (1a) [31,32,33] and (1b) [33, 34, 35, 36] are the main protonation reactions given in literature to describe the incorporation of water, generally into oxygen-deficient perovskites ceramics.

$$H_2O_{(g)} + V_O^{\bullet\bullet} \leftrightarrow 2H_i^{\bullet} + O_O \quad \textbf{(1a)}$$

$$H_2O_{(g)} + V_O^{\bullet\bullet} + O_O \leftrightarrow 2(OH_O^{\bullet}) \quad \textbf{(1b)}$$

They lead to a global reaction (1c) as given by Deng *et al.*[37]

$$H_2O_{(g)} + V_O^{\bullet\bullet} + O_O \leftrightarrow 2H \cdots O_O^{\bullet} \quad \textbf{(1c)}$$

However, this last assumption is not always confirmed and it is not trivial to determine the nature or position of protons in oxides [24,27,33,38,39]. Also, the dissociation mechanism of water molecules has not yet been well understood in the literature [27].

In the case of apatite material, which can present oxygen interstitials or vacancies, three other protonation reactions can be suggested [19,20] involving oxygen interstitial:

$$H_2O_{(g)} + O_O \leftrightarrow OH_O^{\bullet} + OH_i' \quad \textbf{(2)}$$

$$H_2O_{(g)} + O_i'' \leftrightarrow 2\,OH_i' \quad \textbf{(3)}$$

$$H_2O_{(g)} + 2\,O_O \leftrightarrow 2\,OH_O^{\bullet} + O_i'' \quad \textbf{(4)}$$

It is possible to evaluate the amount of water dissociated into the host structure of the material by TGA, which is the most common method to measure the proton amount in oxides [25,26,27,29,40]. The total weight loss observed can reveal the departure of free water, chemically bounded water and hydroxides below 600°C, and the presence of “protonic” species inside the host structure (denoted as bulk “protonic” species) above this temperature. However, the TGA analysis does not allow determining the H content as well as the neutron measurements does [25,26,27,29]. The variation of mass linked to the protonation or the deprotonation of materials is usually very low (less than 1% in weight). Thus the characterization of protonated materials by TGA method requires starting samples pure and dense, to avoid an overestimation of the mass loss caused by impurities or porosity [28].

Despite the proton amount in the host structure is often very low, it is usually sufficient to obtain significant proton conduction through the materials (> 10^{-3} S/cm)[25,27,30]. For instance,

Orera et al. [19] have studied the protonation of a powder of $La_8Ba_2(SiO_4)_6O_2$ lanthanum silicate at 400 °C for 48 h in a tube furnace under flowing nitrogen bubbled through water at room temperature ($pH_2O \approx 0.03$ atm.). As this variation of mass was obtained below 600°C, The low total weight loss of about 0.1% in weight could as well correspond to surface "protonic" species and not bulk.

The aim of this paper is the study of the protonation of Si-based oxyapatite $La_{9.33+x}(SiO_4)_6O_{2+3x/2}$ dense ceramic pellets using a high pressure – high temperature autoclave in order to clarify the protonation mechanism in the oxides. This work corresponds to the first study about the eventual protonation of oxyapatite materials with oxygen sub-stroichiometry (x<0), oxygen-stoichiometry (x=0) and oxygen over-stoichiometry (x>0) at high water pressure (40-50 bars). Besides, an aging test was performed on the most promising sample of initial composition $La_{9.60}(SiO_4)_6O_{2.4}$, in order to study the effect of the duration of the autoclave treatment on the stability and the protonation of the material. Ceramics were characterized by TGA an XRD. Raman spectroscopy was used in order to study the short-range structure according to previous procedure [17,41,42]. The proton insertion and its distribution/effect in the apatite structure have never been studied using Raman spectroscopy. We discuss here the Raman signature of the large lanthanum oxide channels before and after exposition to high water pressure.

2. Experimental

2.1 Powder synthesis and sintering

Powders of oxyapatite of general formula $La_{9.33+x}(SiO_4)_6O_{2+3x/2}$ (x=-0.2,0,0.27) were synthetized by solid state route from hexagonal $La_2O_2CO_3$ and SiO_2 reagents as explained in previous work [43,44]. After attrition milling in ethanol for 2 hours, the mixture was dried, heated at 1200°C for 4 hours and pressed by isostatic pressing into cylindrical bars at 2000 bars for 1 minute. Conventional sintering at 1550°C for 8 hours was used to densify the samples. Finally, the sintered samples were cut using a diamond wire saw in order to obtain dense pellets of 6 mm diameter and 1 mm thickness.

2.2 High water pressure treatments

Ceramic pellets of compositions $La_{9.13}(SiO_4)_6O_{1.7}$ (La913), $La_{9.33}(SiO_4)_6O_2$ (La933), and $La_{9.60}(SiO_4)_6O_{2.4}$ (La960) were wrapped in gold foil and put in an autoclave with

decarbonated water for 84 hours at 550°C and 50 bars. After 12 hours of treatment, the pressure had decreased to 40 bars, that could indicate an eventual incorporation of water in the ceramic pellets. A second autoclave treatment was performed in the same initial conditions at 550°C and 50 bars for 0, 24, 72 and 408 hours, on four pellets of composition La960. The notations La913_X, La933_X and La960_X (with X the duration of the high water pressure treatment in hours and "NP" indicating a non protonated sample) will be used in the following sections for the sake of clarity.

2.3 Characterizations

Microstructural observations of the samples were conducted on a JEOL 7400 FEG-SEM scanning electron microscope. The pellets were polished and thermally etched prior to observation, and a 10nm thin gold layer was sputtered on their surface to prevent charging phenomenon.

Thermogravimetric analyses were performed on pieces of protonated samples in platinum crucible under helium flow of 20 ml/min from 50 to 1000°C with a heating rate of 5°C/min (TG Setsys Evolution 2400, Setaram Instrumentation, Caluire, France). In order to minimize the experimental errors, the data were corrected by subtracting a reference curve obtained for each composition in the same experimental conditions with a non-protonated sample.

Phase purity of the pristine samples was controlled by X-ray powder diffraction on ground pellets at room temperature using $CuK_{\alpha 1}$ radiation in the 2θ range 10–60° with a step of 0.014° and exposure time of 87 s per step (D8 advance diffractometer, Bruker, Germany).

Refinements of cell parameters were done in the space group $P6_3/m$ following the Rietveld method [45] using Jana2006 software [46]. XRPD intensities were collected in the 2θ range 15–100°, with a step of 0.014° and exposure time of 261 s per step (D8 advance diffractometer, Bruker, Germany). The model used for these refinements comes from the work of Iwata *et al.* [12]. The continuous background was modelled with Legendre polynomial function and the peak profiles were represented by pseudo-Voigt functions.

Room temperature Raman spectroscopy was performed on the surface of samples before and after high water pressure treatment using a LabRam HR800 (Horiba Jobin-Yvon,) at the 514 nm wavelength in the single mode. The laser spot diameter at the focus point was about 2 micrometers (x100 Olympus long working distance objective) and the power was typically about 1 mW at the sample.

Raman mapping has been done using a T64000 Horiba Jobin-Yvon spectrophotometer at the 514 nm wavelength, in the single mode. A 50LWD objective has been used in the backscattering mode. With both spectrophotometer, the spectra were averaged on the area of the bands between 130 and 600 cm^{-1} using LabSpec software. Each spectrum was decomposed into a sum of Lorentzian functions (corresponding to the refined bands [17,41,42]) using FOCUS software [47].

3. Results and discussion

3.1 Characterization of the non-protonated pristine ceramics

X-ray powder diffraction patterns show in Figure 1 that oxyapatite samples synthetized in this study exhibit a high purity, with only small amount of secondary phase $La_2Si_2O_7$ (JCPDS 81-0461) in La913 and La933. All sintered samples had a relative density higher than 98.5%.

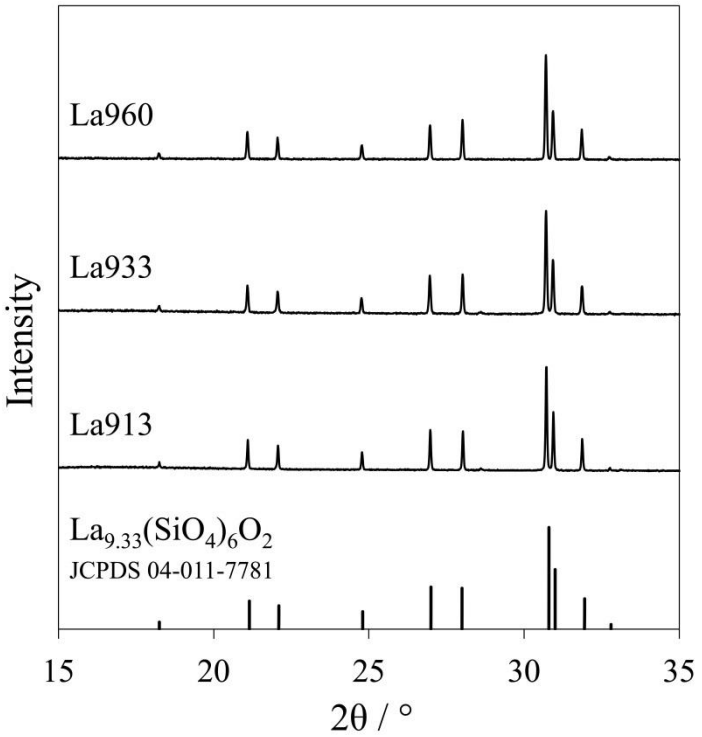

Figure 1 : X-ray diffraction patterns for powdered oxyapatite ceramics of chemical composition $La_{9.13}(SiO_4)_6O_{1.7}$ (La913), $La_{9.33}(SiO_4)_6O_2$ (La933) and $La_{9.60}(SiO_4)_6O_{2.405}$ (La960) compared with the standard $La_{9.33}(SiO_4)_6O_2$.

The average grain size shown in SEM micrographs of the pristine samples [43] is about a few micrometers, with a grain size slightly higher for oxygen deficient sample as discussed in a previous work [17,43,44,48]. This quite large size should be favorable for the incorporation of protonated species, as discussed by Pasteris *et al.* in the temperature study of the $Ca_{10}(PO_4)_6OH$ system [49]. They conclude that the smaller the crystallites, the higher the atomic disorder is, thus making the incorporation of OH^- ions less energetically favorable. This shows that it is very important to get large grains for the optimization of the protonation step, and also to limit grain boundary effects.

Thermogravimetry method is very sensitive to detect traces of volatile species such as water (mass losses before 150°C), hydroxides (mass losses before 400°C.) and carbonates (mass losses before 1000°C). Before protonation, the weight loss of samples was measured twice during a heating up to 1200°C. The mass loss of the unprotonated pellet was about 0.1% for the first heating cycle and 0.05% for the second one. There is no water or carbonate adsorbed at the surface of the sample, as no mass loss occured at low temperature. Also, there was no oxygen loss due to eventual reduction of material under helium atmosphere at high temperature.

A Raman spectroscopy study of the pristine samples was used to determine the bands which are the signature of the high pressure treatment. A typical Raman spectrum of oxyapatite is presented in Figure 2(a), decomposed into a sum of Lorentzian functions using FOCUS software [47] according to previous procedure [17]. The corresponding calculated bands [17,41,42] are given in Table 1. In this work we focus our attention on the wavenumber range below 600 cm^{-1} which is mostly affected by high pressure treatment.

Modes Au, Ag, Eg and Eu given in Table 1 are assigned to the vibrations of oxygen O5 in the large tunnels of oxyapatite structure. These modes were described by Smirnov *et al.* [42] in the case of Sr-doped oxyapatite $La_8Sr_2(SiO_4)_6O_2$ thanks to *ab initio* calculation. The data presented in Table 1 result from a projection of Smirnov's results in the case of compounds $La_{9.33+x}(SiO_4)_6O_{2+3x/2}$.

According to the principle of mutual exclusion in the case of centro-symmetrical structure, modes Ag and Eg are Raman active while modes Au and Eu are IR active. However, bands attributed to modes Au and Eu can be observed in oxyapatite Raman spectra [17,41,42,44], meaning that real symmetry of the large tunnels of oxyapatite is slightly different from the perfect symmetry. Béchade *et al.* [17] showed these modes are affected by the change

of oxygen stoichiometry (insertion of interstitial oxygen in the large tunnel of the structure involving a proposed push-pull mechanism [14,17]).

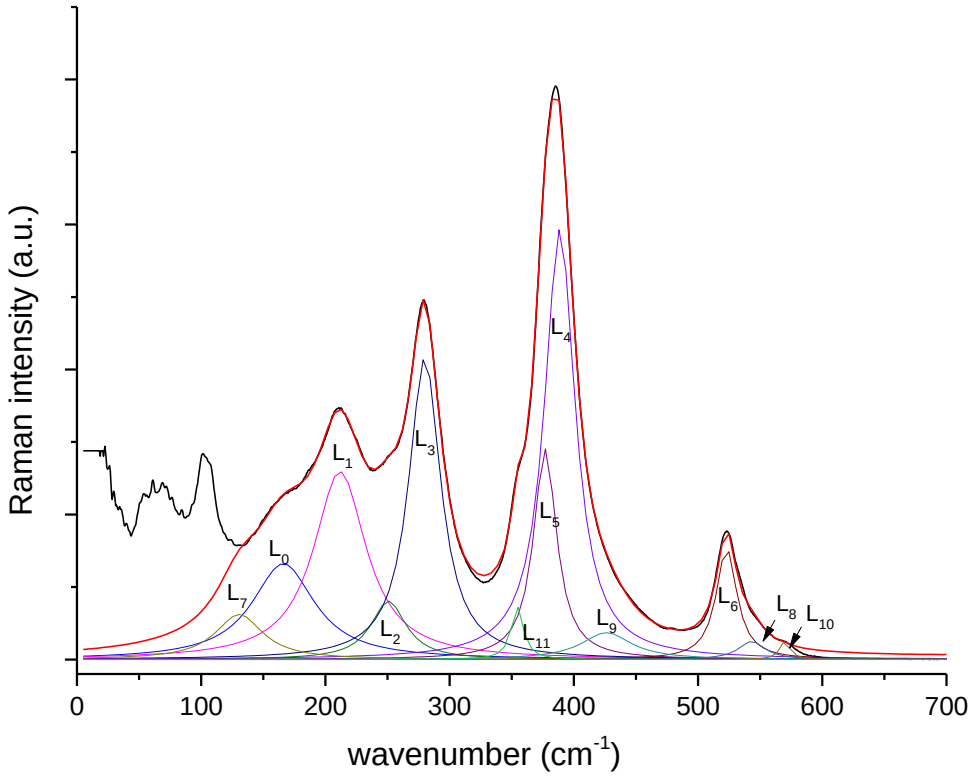

Figure 2: a) Decomposition of the spectrum of oxyapatite (example of La960_NP) at low wavenumbers (from 100 to 600 cm^{-1}).

Table 1: Attribution of the Raman vibration bands refined for the compounds $La_{9.33+x}(SiO_4)_6O_{2+3x/2}$ [17,41,42].

Lorentzian	Raman wavenumber (cm^{-1})	Attribution
L7	135	Lattice modes
L0	180	$La2\text{-}O_{(SiO4)}$ vibrations
L1	213	
L3	276	
L4	393	Symmetric bending mode of SiO4 (ν_2) and $La2\text{-}O_{(SiO4)}$ vibrations
L5	372	
L6	523	Asymmetric bending mode of SiO4 (ν_4)
L8	543	
L9	430	Eg mode: Vibration of O5 oxygen in the xy plane

L10	570	Eu mode: Vibration of O5 oxygen in the xy plane
L11	355	Ag mode: Symmetric vibration of O5 oxygen in the direction parallel to z
L2	250	Au mode: Antisymmetric vibration of O5 oxygen in the direction parallel to z

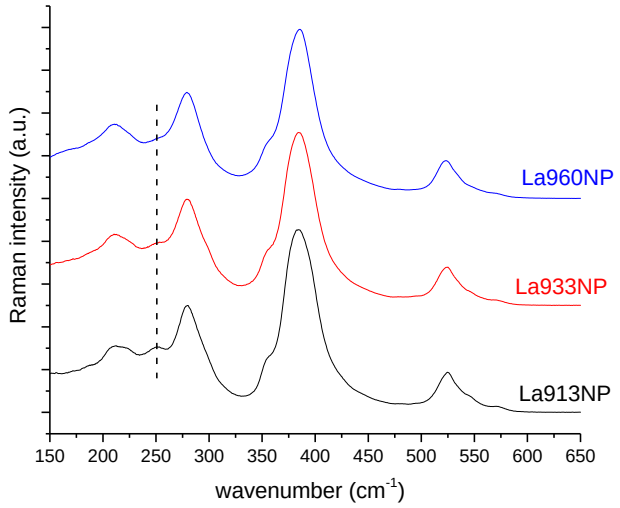

Figure 5: Raman spectra obtained on non protonated samples La913, La933 and La960.

Figure 3 evidences the stoichiometry effect by showing the comparison of Raman spectra measured on samples La913_NP, La933_NP and La960_NP before autoclave treatment. The band which is the most affected by the change of stoichiometry is the Lorentzian noted L2 related to the so-called Au mode. A significant increase of its full width at half maximum (FWHM) can be observed as shown in table 2. This trend can be explain by the creation of an important disorder inside the large channels due to the incorporation of anions in the oxyapatite structure, as reported by other works [9,11,13,14,17,18].

Table 2: Refined widths at half-height w_α in cm^{-1} of Lorentzians Lα (with α = [0-2]) in the case of unprotonated samples La913_NP, La933_NP, La960_NP.

	La913_NP	La933_NP	La960_NP

FWHM (L2) (cm^{-1})	29.23	31.37	34.29

3.2 Composition effect on the protonation of the ceramics

Thermogravimetric analyses performed on oxyapatite samples of different compositions after autoclave treatment (84h/550°C/40bars) are showed in Figure 4. One can notice that after being exposed to high water pressure, all the samples exhibit a mass loss between 100 and 1000°C. Thus the autoclave treatment seems to have affected the material in all cases. Furthermore, two different mass losses are noticeable for each sample: from 100°C to 600°C and from 600°C to 1000°C. Colomban *et al.* [25,26,27] showed that, in the case of perovskite-type materials after autoclave treatment, a mass loss observed while heating a protonated sample below 600°C corresponded to surface "protonic" species while a mass loss happening above 600°C corresponded to volume "protonic" species. In the case of a proton-conducting electrolyte for SOFC application, the involved species must be located in the volume/bulk of the material.

Mass losses observed while heating the material above 600°C are about 0.09%, 0.11% and 0.20% for samples La913_84, La933_84 and La960_84 (Table 3). Thus, the higher the oxygen stoichiometry, the larger the total mass loss is. As a comparison, Orera and Slater [19] observed a mass loss of about 0.4% above 600°C on a sample of composition $La_6Tb_4(GeO_4)_6O_3$ after an autoclave treatment of 48 hours at 200°C and 15 bars. One may note that Orera and Slater [19] used samples are in the form of powder, contrary to our work which involves dense samples (d_{rel}>98.5%). This is important in so far as the density of the sample is a key parameter for water incorporation in the material. Indeed, Colomban *et al.* [27] show that the relative density must be higher than 94% for the samples in order to promote insertion of water in the volume of the material (instead of the surface). Furthermore, GeO_2 solubility in water is several orders of magnitude higher than that of SiO_2 and partial hydrolysis may have happened in Ge-based oxyapatite $La_6Tb_4(GeO_4)_6O_3$, leading to an increase of the total mass loss.

The studies about the protonation of oxides under high water pressure at moderate temperature (600°C) are very scarce in the literature, thus it is not possible to compare the data collected in this work with other data collected in the literature.

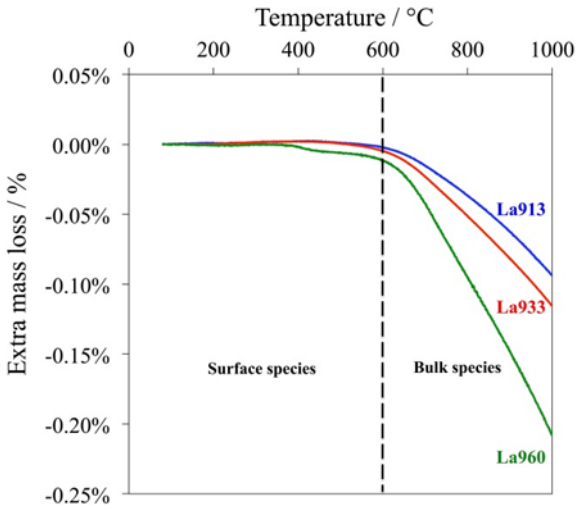

Figure 4: TGA performed on oxyapatite samples La913, La933 and La960 after autoclave treatment at 550°C/40 bars/84h. Data are corrected by subtraction of the signal monitored for unprotonated samples La913, La933 and La960 respectively.

Table 3: Mass losses of protonated samples observed by thermogravimetry. Comparison with $La_6Tb_4(GeO_4)_6O_3$ [19]

Sample	Autoclave treatment	Total mass loss 100°C to 1000°C (%)	Mass loss above 600°C (%)
La913_84	84h/550°C/40bars	0.09	0.09
La933_84	84h/550°C/40bars	0.12	0.11
La960_84	84h/550°C/40bars	0.21	0.20
$La_6Tb_4(GeO_4)_6O_3$	48h/200°C/15bars	1.76	0.40

In these samples, the composition La913 (with oxygen vacancies, $V_O^{\bullet\bullet}$) is the one that shows the lowest mass loss. Thus, protonation mechanism by oxygen vacancies as proposed in equations (1a), (1b) and (1c) does not seem to be the predominant protonation mechanism in the case of oxyapatite.

On the contrary, composition La960 exhibits the larger mass loss, so high initial oxygen stoichiometry seems to promote protonation of oxyapatite. This is a good agreement with the study of Orera and Slater [19,20], who explain the incorporation of protons in Si and Ge-based oxyapatites, as previously presented in equations (2), (3) and (4).

Contrary to equations (1a, b and c), these mechanisms don't involve oxygen vacancies but oxygen atoms of the network $\boldsymbol{O_O}$ and interstitial oxygen atoms $\boldsymbol{O_i''}$. They are leading to the formation of hydroxide ions on the sites of oxygen of the network ($\boldsymbol{OH_O^\bullet}$), interstitial hydroxide ions ($\boldsymbol{OH_i'}$) and additional interstitial oxide ions $\boldsymbol{O_i''}$.

As the apatite samples were exposed, to very extreme conditions of temperature and pressure in this work (550°C, 40-50 bars), one can also consider reaction (5). This equation describes the dissociation of water and its incorporation in the structure of the material under the influence of high pressure and temperature. This results in the formation of two interstitial protons and an interstitial oxygen atom.

$$H_2O_{(g)} \leftrightarrow 2\ H_i^\bullet + O_i'' \qquad \textbf{(5)}$$

It is to note that in all cases (equations (2) to (5)), protonation of oxyapatite may induce the incorporation of oxygen on interstitial site, in the form of $\boldsymbol{OH_i'}$ or $\boldsymbol{O_i''}$.

On a structural point of view, in the case of protonated samples La913_84, La933_84 and La960_84, it was not possible to refine the width at half-height of the Lorentzians, because the band at 250 cm^{-1} (attributed to the Au mode) forms a very small shoulder on the massif at 280 cm^{-1} and because this massif is shifted to the lower wavenumbers. However, as seen in Figure 5, the bands Ag and Eg are modified as compared to the ones measured in non-protonated samples. For example, the band at 440 cm^{-1}, which is attributed to Eg mode, is more visible on spectra of protonated samples (La913_84, La933_84 and La960_84) than on the spectra of the unprotonated samples (La913_NP, La933_NP and La933_NP in Figure 3). This is in agreement with previous study of Orera *et al.* [19,20] and this assumes that La-O bonds close to the channel are modified.

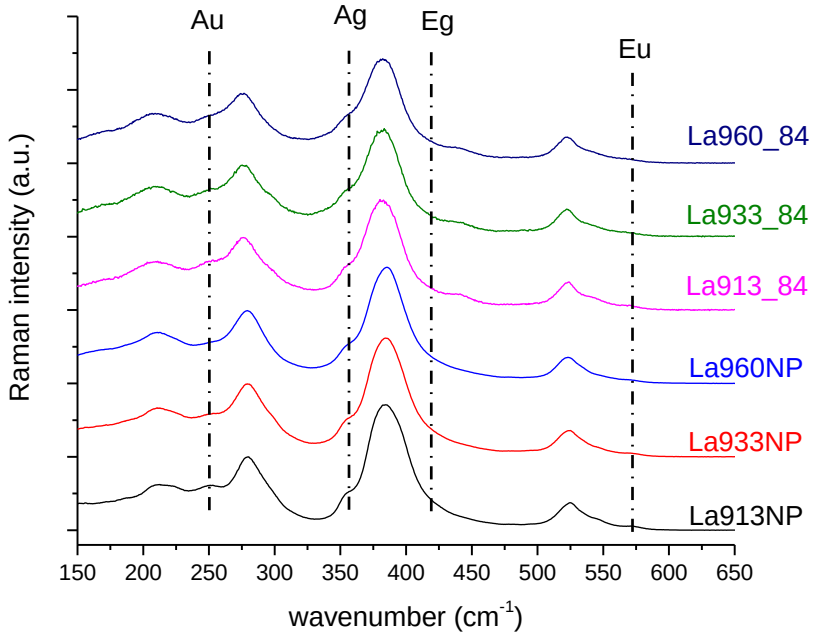

Figure 5: Raman spectra obtained with an incident wavelenght of 514.5 nm samples La913, La933 and La960 protonated 84h at 500°C and 40bars.

Moreover we recorded wide spectral range (100-5000 cm^{-1}) Raman spectra on samples La913_84, La933_84 and La960_84 and on a pristine sample (Figure 6). On one hand, a large luminescence band was observed between 1000 and 4500 cm^{-1} (centred approximately at 2500 cm^{-1}) in the case of protonated samples La913_84 and La933_84 but not in the case of protonated sample La960_84.

This band seems to be similar to the one observed in the case of perovskite materials by Colomban et al. [24,27,28,29], in this point of view we can suppose that this phenomenon may be due to the creation of electronic defects in relation to water exposure (proton/oxygen diffusion). In the case of La960_84 sample, the lack of intrinsic oxygen vacancies should be noted and may induced different phenomena[44].

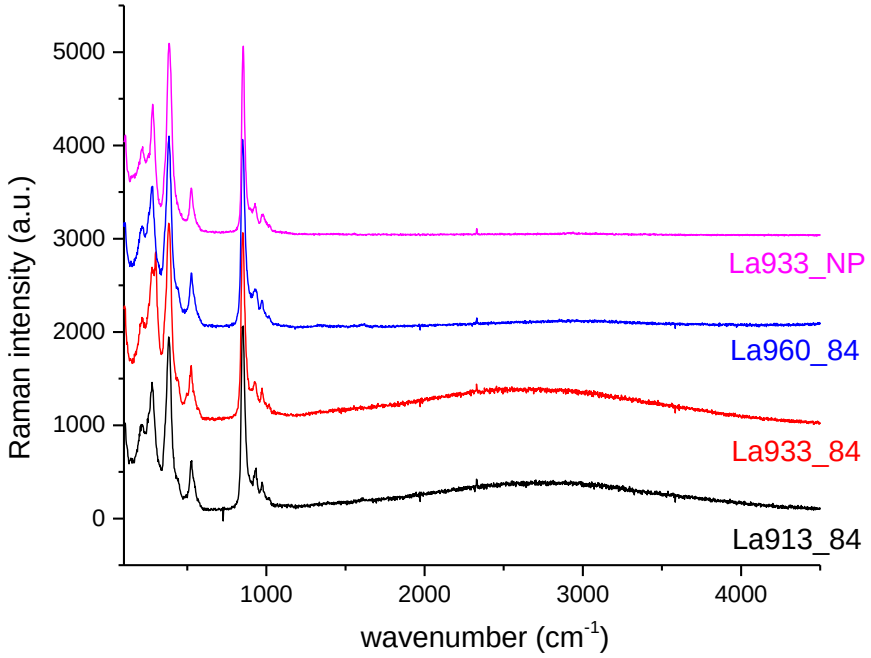

Figure 6. Raman spectra monitored in spectral range 100-4500 cm^{-1} (λ_{inc} = 514.5 nm) on protonated oxyapatite samples La913_84, La933_84, La960_84 and on unprotonated sample (La933_NP) for comparison.

As an illustration, Raman mapping performed on the fresh surface of an unprotonated sample La913_NP and a protonated sample La913_84 is shown on Figure 7. Studied areas are represented by orange rectangles on the optical microscopy images. Raman picture is reconstructed on the integrated intensity of the area of the wavenumber range between 1100 and 4000 cm^{-1} in both cases. The intensity has been normalizing between 0 and 100 for the two maps to be able to compare both images. Protonated sample map clearly evidence that luminescence phenomenon is not homogeneous on the surface of the sample because of the strong contrast of colour related to the huge difference of the integrated intensity of the band under study whereas the non-protonated sample map evidence no luminescence phenomenon at the entire surface (only one colour evidence a very low intensity of the integrated intensity of the band under study). Areas of the mapping where the intensity of the band is the highest (in red/yellow) seem to correspond to white areas on the optical microscopy images. Such an inhomogeneity of the luminescence phenomenon could be due to an inhomogeneity of the microstructure or structure of the material. As shown on Figure 7, all grains are not affected and it could be possible that grain orientation is an important parameter. However, the areas where the intensity is the highest (in red/yellow) have dimensions higher than 100 μm^2, which

is much higher that the grain size. So, further investigation is necessary to understand this phenomenon.

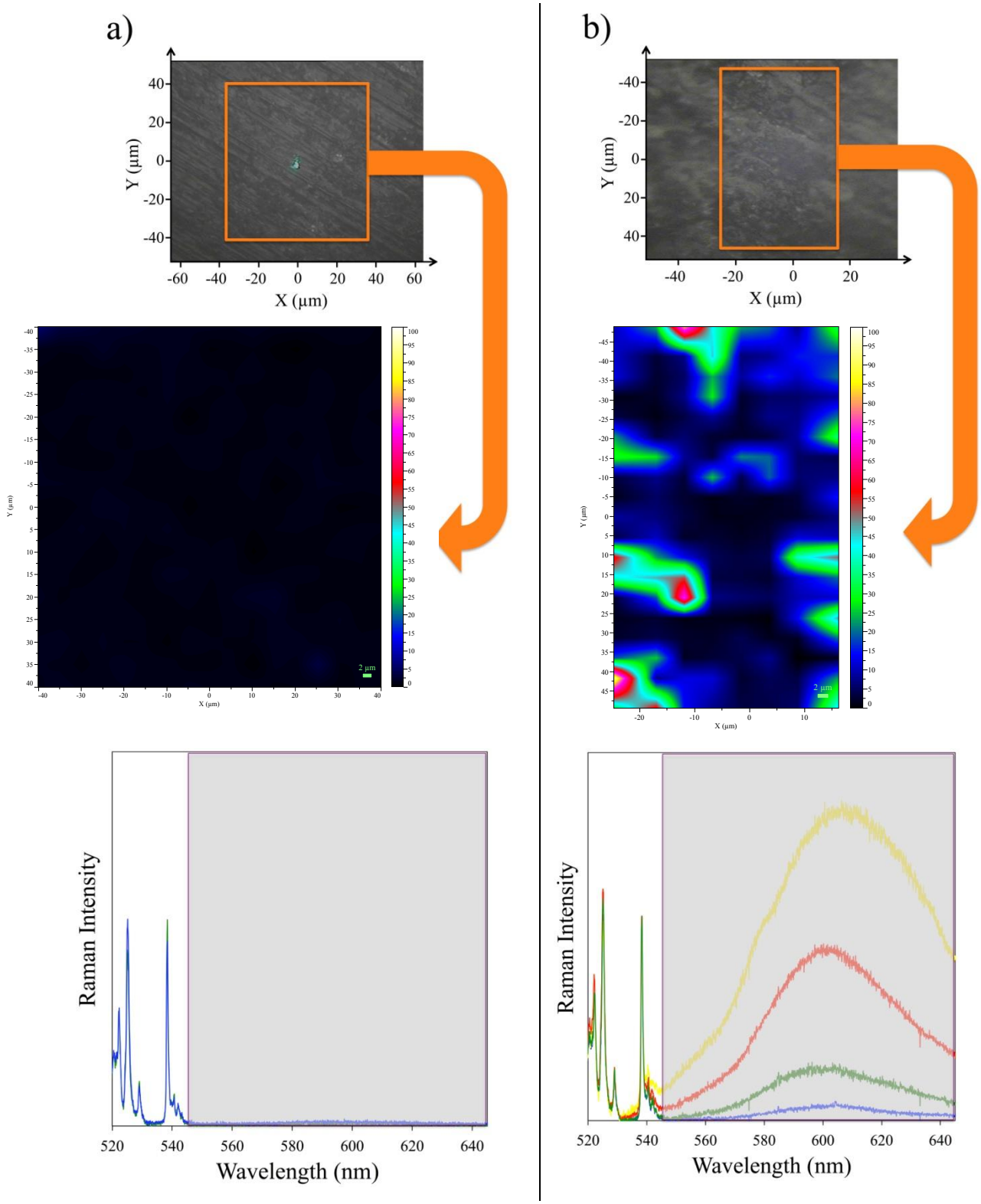

Figure 7: Mapping (a) of La913_NP (b) La913_84, optical view of the mapped area and corresponding representative spectra

3.3 Protonation of La960

Samples with the composition La960 being the most favorable in the incorporation of protonic species, a further study was conducted to see the influence of longer time treatments in autoclave. Pellets were placed in the autoclave at 550°C and 50 bars for durations of 24h, 72 and 408h. The thermogravimetric curves of the protonated samples are given in Figure 8. Mass losses observed while heating the material above 600°C, given in Table 4, are about 0.14%, 0.19%, 0.66% for samples La960_24, La960_72, La960_408 respectively. In this series of samples, there seems to be more surface protonic species than in the previous section, characterized by a larger mass loss in the range 100°C-600°C. Concerning volume species, the mass loss increases with the protonation time, showing some kinetic effect to the phenomenon.

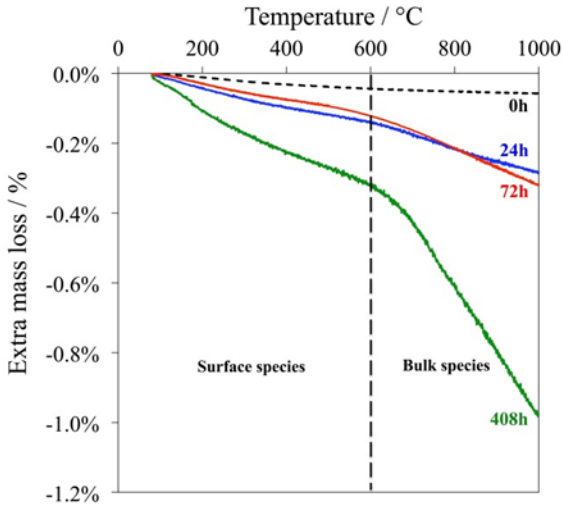

Figure 8: TGA performed on oxyapatite samples La960 after autoclave treatment at 550°C/50 bars for 24h, 72h and 408h.Data are corrected by subtraction of the signal monitored for unprotonated samples.

Table 4: Mass losses of La960 samples protonated for different durations observed by thermogravimetry.

Sample	Autoclave treatment	Total mass loss 100°C to 1000°C (%)	Mass loss above 600°C (%)
La960_24	24h/550°C/50bars	0.28	0.14

La960_72	72h/550°C/50bars	0.32	0.19
La960_408	408h/550°C/50bars	0.98	0.66

The microstructure of the polished and thermally etched pellets before and after the protonation process is shown in Figure 9. The unprotonated sample, Figure 9a, shows a grain size distribution of 0.5 µm to 2 µm with no porosity. After 24h in the autoclave, the microstructure of the pellet remains largely unaffected (Figure 9b). However some striations can be observed on some grains of the sample. They don't seem to be preferentially present on small or big grains but randomly distributed. The sample protonated during 72 hours (Figure 9c) is characterized by a visible surface corrosion and striations on the whole sample. After 408h of autoclave treatment, the microstructure of the sample is widely damaged (Figure 9d). Some gains are so extensively corroded that their boundaries are not visible. Once again, the effect does not seem to be related to the grain size.

However, it is interesting to note that the oxyapatite samples are very stable under those harsh conditions. The pressure values in this work are 2–5 times higher than that required in an industrial use [50]. Although the sample treated during 408 hours broke during the protonation, probably due to a too large modification of the cell parameters, the pellets are still in good condition after protonation. It is not the case with perovskite-based materials, for example, $BaCe_{0,5}Zr_{0,3}Y_{0,16}Zn_{0,04}O_{3-\delta}$, which was damaged after 30 hours of autoclave treatment in much smoother conditions, namely 500°C and 10 bars [28].

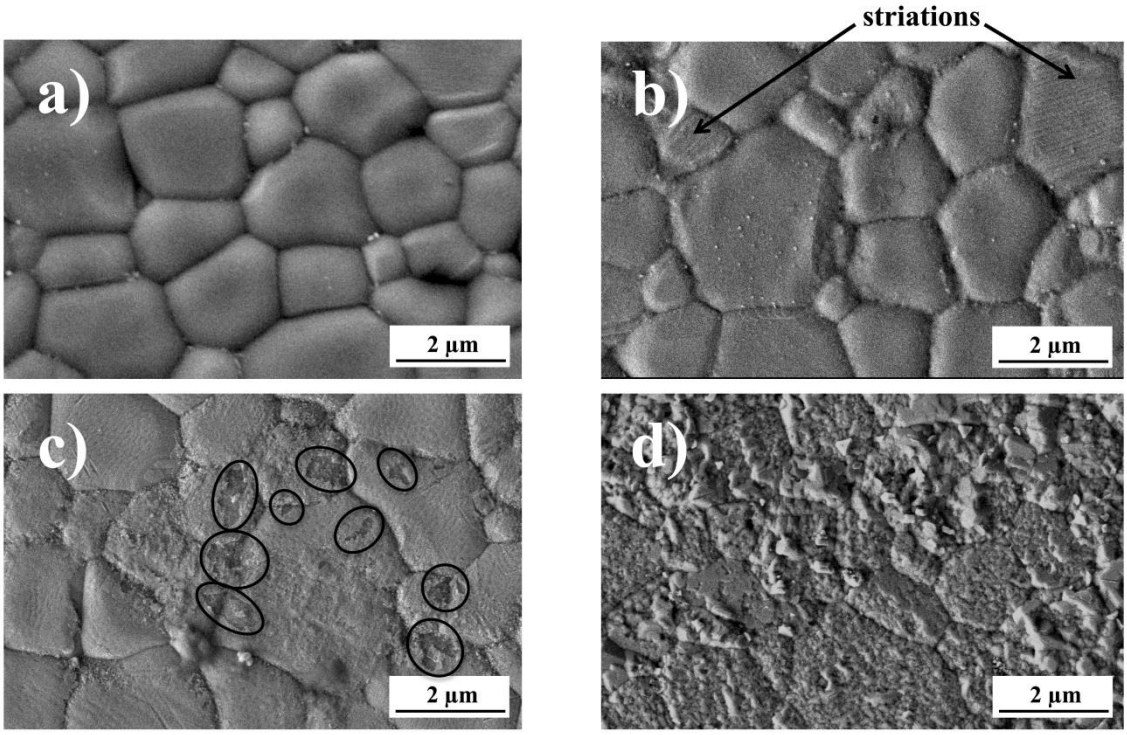

Figure 9: SEM micrographs of the La960 sample after a) 0h, b) 24h, c) 72h and d) 408h of protonation at 550°C and 50 bars. Circles indicate the appearance of a second zone with different contrast.

Rietveld refinement of lattice parameters of sample La960 (Figure 10a) were performed before and after autoclave treatment at 550°C, 50 bars, 72h. This sample was chosen because it had the larger mass loss with no damage of the microstructure. Changes were observed between the diagrams of protonated and unprotonated samples (Figure 10b). Indeed, after autoclave treatment, the full width at half maximum is larger and the peaks' profiles seem asymmetric. After a closer examination, however, the profiles of the peaks corresponding to the plans *(0,0,l)* are not affected. Thus the autoclave treatment seems to induce structural modifications but the *c* direction is not involved (anisotropic structural modification). Furthermore, in the case of the autoclave-treated sample, what seemed to be asymmetry could be in fact modelled using two apatite phases of same symmetry and different lattice parameters (phases named #1 and #2 in Figure 10b).

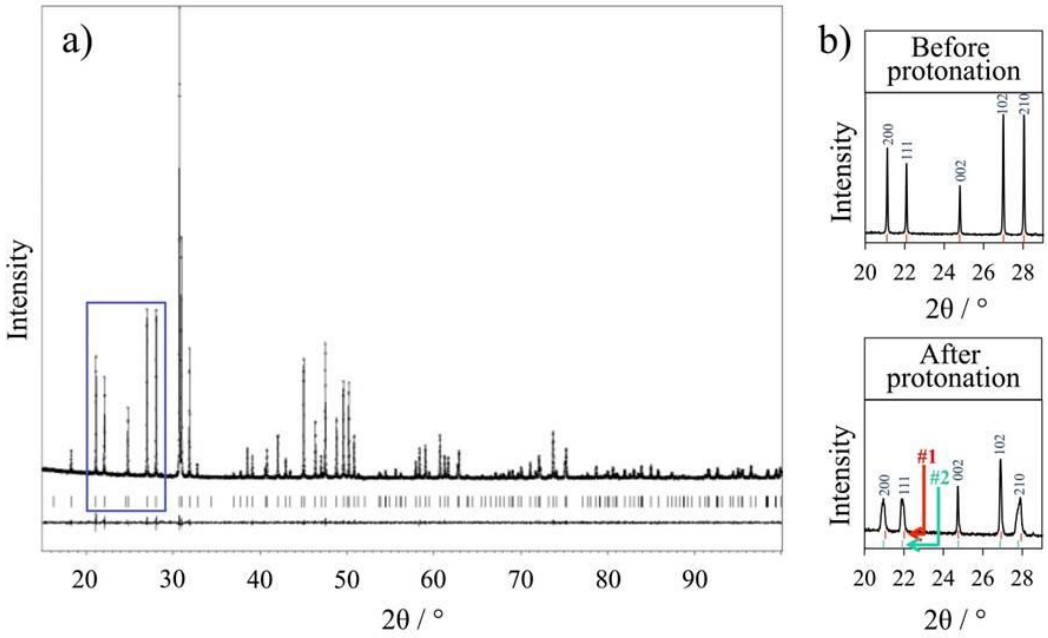

Figure 10: a) Comparison of the observed diffraction pattern (symbol +) with the corresponding calculated pattern (upper solid line) for La960_72. The vertical bars indicate the position of possible Bragg reflections. The difference curve is shown in the lower part of the diagram. The blue square shows the area more specifically analysed in (b). b) Comparison in the 2θ-range [20°-29°] of the XRDP of La960_NP and after protonation at 550°C/50 bars/72h (lower part). #1 and #2 represent two apatite phases with different lattice parameters.

As shown in Table 5, lattice parameters of the non-protonated sample and of phase #1 of the autoclave-treated sample are similar ($a = b \approx 9.7$ Å and $c \approx 7.2$ Å). On the contrary, lattice parameters a and b of phase #2 are larger ($a = b \approx 9.8$ Å) while c remains constant, which is in good agreement with an anisotropic structural modification. The volume of the unit cell in phase #2 of the autoclave-treated sample ($V \approx 597.69$ Å^3) is much larger than the one of the non-protonated sample ($V \approx 587.69$ Å^3). The values reported in literature ($V \approx$ 587.77 Å^3 and 587.08 Å^3 for $La_{9.33}(SiO_4)_6O_2$ and $La_{10}(SiO_4)_6O_3$ respectively [9], $V \approx 588.93$ Å^3 and 588.94 Å^3 for $La_{9.16}(SiO_4)_6O_{1.75}$ and $La_{9.33}(SiO_4)_6O_2$ respectively [51]) show that the volume of the unit cell is not as much affected by the oxygen content and that the variation of the results (for the composition $La_{9.33}(SiO_4)_6O_2$) between the two studies is about 1 Å. As a comparison, the variation of the unit cell volume, between the non-protonated sample and the phase #2 of the autoclave-treated sample, is about 10 Å.

Such a large increase of the unit cell volume, correlated with the increase of the a and b lattice parameters, may indicate an enlargement of the channels of the apatite structure in

the plan (x,y). However, this structural change is not homogeneous in the whole sample as the initial apatite phase #1 remains in the protonated sample. This could mean that the protonation was not completely achieved in the "heart" of the ceramic. Indeed, insertion of protons and oxygen ions in the structure of the material (forming "bulk species") takes place in an area close to the surface of the sample and a long step of diffusion of the defects is required to obtain homogeneous protonation [27]. The same effect can be observed in ceramics when using some sintering aid. For example, Bencan et al. showed the incorporation of Ge in $KNaNbO_3$ ceramics, with the formation of two phases of different unit cell volumes [52].

Table 5: Lattice parameters and unit cell volume calculated by Rietveld refinement for sample La960 before autoclave treatment (GoF=2.12, Rp=6.51%, Rwp=9.55%) and after protonation at 550°C/50 bars/72h (GoF=1.20, Rp=3.70%, Rwp=4.9%).

	a, *b* (Å)	*c* (Å)	*V* (Å^3)
La960_NP	9.7204 (1)	7.1820 (1)	587.69 (1)
La960_72 phase #1	9.7432 (4)	7.1864 (5)	590.81 (4)
La960_72 phase #2	9.8139 (3)	7.1658 (4)	597.69 (4)

The Raman spectra of the La960 samples after different durations of autoclave treatment are shown in Figure 11. Once again, it was not possible to refine the width at half-height of the Lorentzians at 250 cm^{-1} (attributed to the Au mode). The shifting of the massif at 280 cm^{-1} to the lower wavenumbers is well visible in this figure, where the bands at 280 and 380 cm^{-1} (represented by orange lines) are translating to lower wavenumbers as the duration of the autoclave treatment increases. Thus, positions of Lorentzians L3 (corresponding to the band at 280 cm^{-1}), and L4 and L5 (corresponding to the band at 380 cm^{-1}) were refined and noted x_{L3}, x_{L4} and x_{L5} respectively in Table 6. One can note that x_{L3}, x_{L4} and x_{L5} decrease from 279.93 to 276.85 cm^{-1}, from 388.71 to 385.88 cm^{-1} and from 376.93 to 374.93 cm^{-1}, respectively, while the duration of autoclave treatment rises from 0 to 408 hours. As explained in Table 1, L3 is attributed to the La2-$O_{(SiO4)}$ vibration mode and L4 and L5 are attributed to the symmetric bending mode of SiO_4 (ν_2) and to the La2-$O_{(SiO4)}$ vibration mode. Thus, the shift of the Lorentzians' positions to lower wavenumbers values could be due to the increase of the average length of bond La2-$O_{(SiO4)}$. This confirms that a structural change occurs inside the large channels, which seem to be enlarged while the duration of the autoclave treatment increases. This is also in good agreement with lattice parameters

refinements (Table 5), and seems to confirm the incorporation of protonic species into the material.

Furthermore, FWHM of Lorentzians L1 and L3, attributed to the vibrations La2-$O_{(SiO4)}$, are higher in the case of samples La960 aged in autoclave compared to La960_NP. Indeed, FWHM(w_1) and (w_3) are equal to 51.37 and 31.18 cm^{-1}, respectively, for sample La960 before aging test, and are about 65-67 and 37-39 cm^{-1}, respectively, for samples La960 aged in autoclave. This change can be linked to the creation of a significant disorder in the La2-$O_{(SiO4)}$ distances at the periphery of the large tunnels of oxyapatite, which is also consistent with the incorporation of protonic species inside the structure.

Moreover, one can notice on Figure 11 that the longer the autoclave treatment, the more visible the vibrational mode Eg at 440 cm^{-1} is. As this mode is Raman active, this could mean that the protonation process induces a symmetry change inside the large tunnels of the oxyapatite structure, leading towards ideal theoretical symmetry. This seems to confirm that a symmetry change happens inside the large channels of the oxyapatite structure during the protonation process: the symmetry may evolve towards ideal theoretical symmetry as the autoclave treatment duration increases.

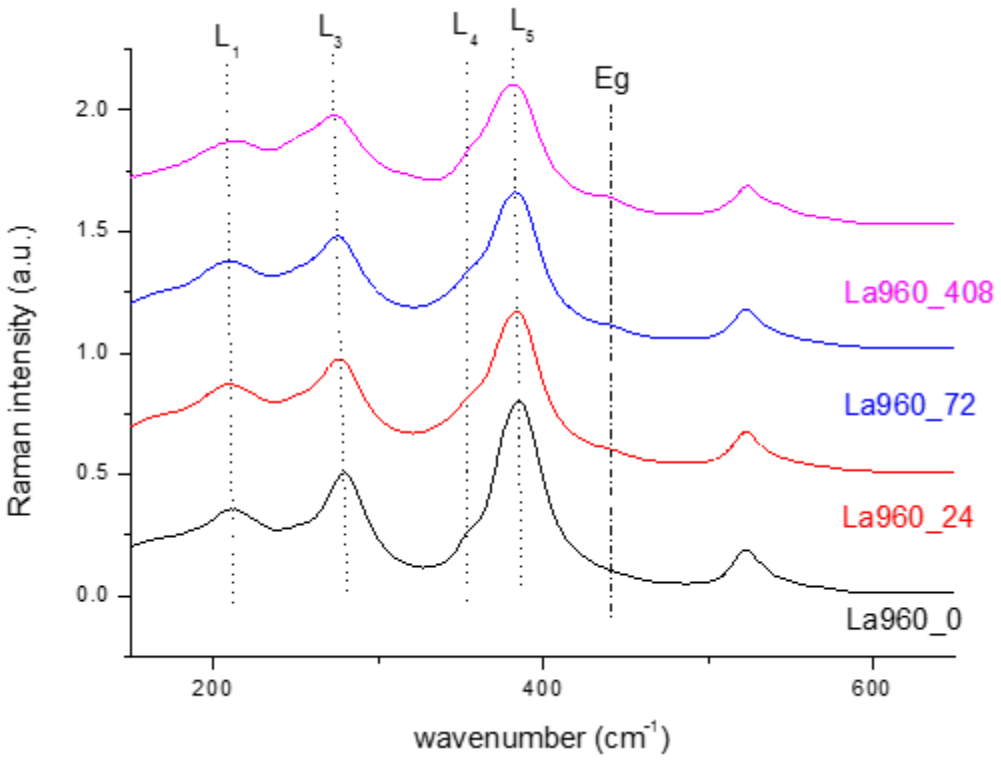

Figure 11: Raman spectra on samples La960 after autoclave treatment of 0h, 24h, 72h, and 408h at 550°C/50 bars.

Table 6: Refined FWHM and positions (FWHM(L_α) and $x_{L\alpha}$ respectively, in cm^{-1}) of Lorentzians Lα (with α = [1-5]) in the case of La960 aged by autoclave treatment (550°C/50 bars/ 0h, 24h, 72h, 408h.

		La960_NP	La960_24	La960_72	La960_408
Frequency (cm^{-1})	x_{L3}	280	277	276	277
	$x_{L4}x_4$	389	386	386	386
	x_{L5}	377	375	375	375
FWHM (cm^{-1})	FWHM(L_1)	51	65	65	67
	FWHM(L3)	31	37	40	37

4. Conclusion

In this work, we have investigated for the first time the protonation of pure and dense samples of initial compositions $La_{9.13}(SiO_4)_6O_{1.7}$ (oxygen sub-stoichiometric), $La_{9.33}(SiO_4)_6O_2$ (oxygen stoichiometric), and $La_{9.60}(SiO_4)_6O_{2.4}$ (oxygen over-stoichiometric), exposed at a temperature close to the expected operating condition (550°C) under high water pressure. The effects of initial composition and protonation time were studied. It was shown that autoclave treatment induces microstructural and structural changes in the samples due to the insertion of protonic species in the volume of the material. According to thermogravimetric measurements, the over-stoichiometric composition La960 showed the highest mass gain after 84 hours of autoclave treatment at 550°C and 40 bars, probably due to the presence of interstitial ions leading to OH_i' or a combination of $OH_O^\bullet + O_i''$ defects, contrary to perovskite material where oxygen vacancies are favored.

Additional tests performed on composition $La_{9.60}(SiO_4)_6O_{2.4}$ brought out that the inserted species content in oxyapatite increases when protonation time rises. SEM surface analysis of sample La960 shows the creation of striations on some grain surface after 72 hours of treatment and the increase of surface corrosion with treatment duration. After a long duration of treatments (408 hours at 550°C/50 bars), the samples are broken in several parts.

An increase of the cell volume in the (a,b) plane, corresponding to an enlargement of the tunnels of the apatite structure were observed, as well as an increase of the disorder at the periphery of the tunnels. These observations confirm that protonic species were incorporated

into the material and show that they may be located mainly inside the large tunnels of the apatite structure. The proton insertion in the structure of oxyapatite may induce the creation of active centres, which may instigate the fluorescence phenomena observed in this study.

Further investigations may be carried out in order to determine the nature of these protonic species as well as the time required to obtain homogeneous protonation for oxyapatite materials. Then, electrical characterizations of apatite *in-situ* autoclave coupled Raman microscopy could provide also interesting additional information to determine the effect ox protonation on the conduction properties in oxyapatites.

Aknowledgments

The authors wish to thank Julie Cornette, Richard Mayet and Pascal Munsch for their support concerning Raman spectroscopy, X-ray diffraction and autoclave experiments.

References

[1] N.Q. Minh, Solid State Ionics 174 (2004) 271 – 277

[2] O. Yamamoto, Electrochimica Acta 45 (2000) 2423 – 2435

[3] F.M.B. Marques, V.V. Kharton, E.N. Naumovich, A.L. Shaula, A.V. Kovalevsky, A.A. Yaremchenko, Solid State Ionics 177 (2006) 1697–1703

[4] S. Nakayama, T. Kageyama, H. Aono, Y. Sadaoka, J. Mater. Chem. 5 (1995) 1801–1805

[5] S. Nakayama, M. Sakamoto, J. Eur. Ceram. Soc. 18 (1998) 1413 – 1418

[6] K. Fukuda, T. Asaka, R. Hamaguchi, T. Suzuki, H. Oka, A. Berghout, E. Béchade, O. Masson, I. Julien, E. Champion, P. Thomas, Chem. Mater. 23 (2011) 5474–5483

[7] K. Fukuda, T. Asaka, M. Okino, A. Berghout, E. Béchade, O. Masson, I. Julien, P. Thomas, Solid State Ionics 217 (2012) 40–45

[8] S. Nakayama, A. Ikesue, Y. Higuchi, M. Sugawara, M. Sakamoto, J. Eur. Ceram. Soc. 33 (2013) 207 – 210

[9] H. Yoshioka, J. Eur. Ceram. Soc. 90 (2007) 3099 – 3105

[10] H. Okudera, Y. Masubuchi, S. Kikkawa, A. Yoshiasa, Solid State Ionics 176 (2005) 1473 – 1478

[11] K. Fukuda, T. Asaka, M. Oyabu, D. Urushihara, A. Berghout, E. Béchade, O. Masson, I. Julien, P. Thomas, Chem. Mater. 24 (2012) 4623–4631

[12] T. Iwata, K. Fukuda, E. Béchade, O. Masson, I. Julien, E. Champion and P. Thomas, Solid State Ionics 178, (2007), 1523-1529

[13] J.R. Tolchard, M.S. Islam, P.R. Slater, J. Mater. Chem. 13 (2003) 1956–1961

[14] E. Béchade, O. Masson, T. Iwata, I. Julien, K. Fukuda, P. Thomas, E. Champion, Chem. Mater. 21 (2009) 2508–2517

[15] S. Nakayama, Y. Higuchi, M. Sugawara, A. Makiya, K. Uematsu, M. Sakamoto, Ceram. Int. 40 (2014) 1221-1224

[16] K. Fukuda, T. Asaka, S. Hara, M. Oyabu, A. Berghout, E. Béchade, O. Masson, I. Julien, P. Thomas, Chem. Mater. 25 (2013) 2154–2162

[17] E. Béchade, Thesis, University of Limoges (2008)

[18] L. León-Reina, J.M. Porras-Vázquez, E.R. Losilla, M.A.G. Aranda, J. Solid State Chem. 180 (2007) 1250 – 1258

[19] A. Orera, P.R. Slater, Solid State Ionics 181 (2010) 110 – 114

[20] P.M. Panchmatia, A. Orera, E. Kendrick, J.V. Hanna, M.E. Smith, P.R. Slater, M.S. Islam, J. Mater. Chem. 20 (2010) 2766–2772

[21] J.A. Kilner, J. Druce and T. Ishihara, High-Temperature Solid Oxide Fuel Cells for the 21st Century: Fundamentals, Design and Applications: Second Edition, November 16 (2015), 85-132 (Book Chapter)

[22] T. Norby, J. Chem. Eng. Jpn. 40, (2007), 1166-1171

[23] D.G. Thomas and J.J Lander, J. Chem. Phys.25 (1956), 1136-1142

[24] A. Slodczyk, P. Colomban, S. Willemin, O. Lacroix, B. Sala, J. Raman Spectrosc. 40 (2009) 513–521

[25] P. Colomban, A. Slodczyk, D. Lamago, G. Andre, O. Zaafrani, O. Lacroix, S. Willemin, B. Sala, J. Phys. Soc. Jpn. 79 (2010) 1–6

[26] P. Colomban, A. Slodczyk, Eur. Phys. J. Special Topics 213 (2012) 171–193

[27] P. Colomban, O. Zaafrani, A. Slodczyk, Membranes 2 (2012) 493–509

[28] A. Slodczyk, O. Zaafrani, M.D. Sharp, J.A. Kilner, B. Dabrowski, O. Lacroix, P. Colomban, Membranes 3 (2013) 311–330

[29] A. Slodczyk, M.D. Sharp, S. Upasen, P. Colomban, J.A. Kilner, Solid State Ionics 262 (2014) 870–874

[30] Y. Larring, C. Vigen, F. Ahouanto, M-L. Fontaine, T. Peters, J. B. Smith, T. Norby and Rune Bredesen, Membranes 2 (2012) 665-686

[31] H. Iwahara, Solid State Ionics 86-88 (1996) 9–15

[32] K.J. de Vries, Solid State Ionics 100 (1997) 193 – 200

[33] P. Colomban, Annales de Chimie - Science Des Matériaux 24 (1999) 1–18

[34] A.S. Nowick, Y. Du, Solid State Ionics 77 (1995) 137 – 146

[35] A.S. Nowick, A.V. Vaysleyb, Solid State Ionics 97 (1997) 17 – 26

[36] K.D. Kreuer, Annu. Rev. Mater. Res. 33 (2003) 333–359

[37] S. Deng and Y. Zhang, Phys. Status Solidi B, 253 (2016) 1688-1696

[38] T. Norby, M. Widerøe, R. Gløckner and Y. Larring, Dalton Trans.19, (2004), 3012-3018

[39] P. Colomban, C. Tran, O. Zaafrani, A. Slodczyk, J. Raman Spectrosc. 44 (2013) 312–320

[40] P. Colomban, Fuel Cells 13 (2013) 6–18

[41] E. Rodríguez-Reyna, A.F. Fuentes, M. MacZka, J. Hanuza, K. Boulahya, U. Amador, Solid State Sci. 8 (2006) 168–177

[42] M. Smirnov, S. Sukhomlinov, A. Mirgorodsky, O. Masson, E. Béchade, M. Colas, T. Merle-Méjean, I. Julien, P. Thomas, J. Raman Spectrosc. 41 (2010) 1700–1707

[43] A. Pons, J. Jouin, E. Béchade, I. Julien, O. Masson, P.M. Geffroy, R. Mayet, P. Thomas, K. Fukuda, I. Kagomiya, Solid State Sci. 38 (2014) 150–155

[44] A. Pons, Thesis, University of Limoges (2014)

[45] H.M. Rietveld, J. Appl. Crystallogr. 2 (1969) 65–71

[46] JANA2006 Software. Download website: http://jana.fzu.cz/

[47] Focus, Software Utility for the Creation of Optical Function, Domingos DE SOUSA MENESES, CEMHTI, UPR-CNRS 3079, Orléans. Download website: http://crmht.cnrs-orleans.fr/pot/software/focus.html

[48] E. Béchade, I. Julien, T. Iwata, O. Masson, P. Thomas, E. Champion, K. Fukuda, J. Eur. Ceram. Soc. 28 (2008) 2717-2724

[49]J. D. Pasteris, B. Wopenka, J. J. Freeman, K. Rogers, E. Valsami-Jones, J. A. M. van der Houwen, et M. J. Silva, Biomaterials 25 (2004) 229-238

[50]B. Sala, F. Grasset, O. Lacroix, A. Sirat, K. Rahmouni, M. Keddam, H. Takenouti, D. Goeuriot, B. Bendjeriou, Ph. Colomban, A. van der Lee, J.G. Sanchez, WO2013053858 A1 (18/04/2013) Google Patents, France, 2013

[51] T. Iwata, E. Béchade, K. Fukuda, O. Masson, I. Julien, E. Champion, P. Thomas, J. Am. Ceram. Soc. 91 (2008) 3714–3720

[52] A. Bencan, J. Bernard, J. Tellier, B. Malic and M. Kosec, Microsc. Microanal. 15 (2009) 786-787